Controllable Self-assembly of Carbon Nanotubes on Ammonium Polyphosphate as a Game-Changer for Flame Retardancy and Thermal Conductivity in Epoxy Resin

Yan Xia, Yutong Hong, Li Zhang, Juan Chai, Bingtao Wang, Zhenghong Guo, Juan Li, Siqi Huo*, and Zhengping Fang*

Y. Xia, Y. Hong, L. Zhang, J. Chai, B. Wang, Z. Guo, J. Li, Z. Fang

Institute of Fire Safety Materials, School of Materials Science and Engineering, NingboTech University, Ningbo 315100, China

Email: lijuan@nbt.edu.cn

Y. Xia

Ningbo Dacheng New Material Company Limited, Ningbo 315300, China

S. Huo

School of Engineering, Center for Future Materials, University of Southern Queensland, Springfield 4300, Australia

Email: Siqi.Huo@unisq.edu.au

Keywords: self-assembly, carbon nanotubes, flame retardancy, thermal conductivity, epoxy resin

The optimization of flame retardancy and thermal conductivity in epoxy resin (EP), utilized in critical applications such as mechanical components and electronics packaging, is a significant challenge. Our study introduces a novel, ultrasound-assisted self-assembly technique to create a dual-functional filler consisting of carbon nanotubes and ammonium polyphosphate (CNTs@APP). This method, leveraging dynamic ligand

interactions and strategic solvent selection, allows for precise control over the assembly and distribution of CNTs on APP surfaces, distinguishing it from conventional blending approaches. The integration of 7.5 wt% CNTs@APP_{10} into EP nanocomposites results in substantial improvements in flame retardancy, as evidenced by a limiting oxygen index (LOI) value of 31.8% and achievement of the UL-94 V-0 rating. Additionally, critical fire hazard indicators, including total heat release (THR), total smoke release (TSR), and the peak intensity of CO yield (PCOY), are significantly reduced by 45.9% to 77.5%. This method also leads to a remarkable 3.6-fold increase in char yield, demonstrating its game-changing potential over traditional blending techniques. Moreover, despite minimal CNTs addition, thermal conductivity is notably enhanced, showing a 53% increase. This study introduces a novel approach in the development of multifunctional EP nanocomposites, offering potential for wide range of applications.

1. Introduction

Epoxy resin (EP) is widely utilized across various fields due to its exceptional mechanical strength, adhesive capabilities, chemical stability, and excellent electrical insulation properties[1]. However, its applications, especially in areas that require efficient heat dissipation such as electronic packaging materials, are significantly limited by its low thermal conductivity, which is approximately 0.2 $W \cdot m^{-1} \cdot K^{-1}$[2]. During operation, electronic devices generate heat that cannot be effectively conducted away by EP, leading to overheating, which in turn affects their stability and lifespan[3]. Additionally, EP has a low limiting oxygen index (LOI) of around 19.6%[4, 5], indicating poor flame resistance. This disadvantage is particularly acute in sectors where fire safety is paramount, such as aerospace and high-rise buildings, hence highlighting the limitations of its use[6]. Therefore, it is of great importance to overcome the shortcomings in thermal conductivity and flame retardancy to broaden the application of EP in more demanding sectors.

In response to these challenges, targeted research has been undertaken with the aim of enhancing both thermal and flame-retardant properties without compromising

the performance of EP. A straightforward and scalable strategy involves incorporating thermally conductive fillers and flame retardants directly into the resin matrix[7, 8]. To improve thermal conductivity, materials such as ceramics (e.g., aluminum oxide (α-Al_2O_3), hexagonal boron nitride (h-BN), aluminum nitride (AlN), silicon carbide (SiC))[9], metallic nanoparticles[10], and carbon-based nanomaterials (e.g., carbon nanotubes (CNTs), expanded graphite, graphene) are added to the matrix[11]. However, these materials either require high loading levels (about 50%-80% by mass) to achieve the desired thermal conductivity[12], which can negatively impact the mechanical properties of the resin, or they may aggregate within the polymer matrix, hindering the formation of a conductive network[13]. On the other hand, to enhance flame retardancy, the most common strategy is to blend flame retardants directly into the resin matrix[14]. Studies have shown that synergistic flame retardants, which combine different components, can act in both the gas and condensed phases, demonstrating superior flame retardancy[15]. However, this approach faces common issues, such as inadequate dispersion of flame retardants within the resin, which prevents the necessary quantity of flame retardants from functioning effectively and limits the potential for synergistic effects[16]. More importantly, these drawbacks challenge the control of material properties and the in-depth study of structure-activity relationships, restricting further optimization and application of the materials. Therefore, improving the dispersion of fillers within the matrix and optimize the distribution among different types of fillers to enhance the synergistic effects between different components, ultimately improving the thermal and flame retardant performance of EP.

To overcome these issues, researchers have gradually transitioned from simple blending to employing nanocomposite technology[17], surface functionalization[18], and the fabrication of multifunctional composite fillers[15, 19], aiming to improve the bonding strength and compatibility between thermal fillers, flame retardants, and the EP matrix at the molecular level. These strategies have not only effectively enhanced thermal transfer efficiency and flame retardancy but have also maintained or improved the intrinsic physical and mechanical properties of the materials[20]. For instance, the

functionalization of graphene and CNTs has strengthened their bond with the EP matrix, significantly boosting the thermal efficiency and mechanical performance of the composites without a considerable increase in filler content[21, 22]. It is noteworthy that among the various strategies, the construction of integrated superstructures through self-assembly, which organically integrates different functional components into a unified thermal conductive and flame-retardant filler, is gradually gaining attention[23, 24]. Self-assembly can not only maximize the advantages of each component but can also purposefully regulate the composition and structure of the functional parts, allowing for the customization of the composition and even the structure of the thermal conductive and flame-retardant fillers according to the material's requirements[25, 26]. Despite this, the self-assembly technique has not yet received sufficient focus within the realm of flame retardancy[27-29]. While initial research has demonstrated the impressive potential of self-assembly in enhancing thermal conductivity and flame retardancy, several bottlenecks remain. These include the complexity of the procedures[24], limited functionality[30], low controllability of structures[31], and poor dispersion[32], which can significantly impede the advancement of polymer materials' comprehensive properties. Therefore, it is essential to explore and fully exploit the potential of the self-assembly method in the creation of new materials. By refining the assembly methods, increasing the structural controllability, and expanding the diversity of functional components, it is possible to achieve broader application fields and enhance the level of performance optimization for these advanced materials.

Here, we utilized an ultrasound-assisted self-assembly process, incorporating ligand treatment and strategic solvent selection, to assemble CNTs uniformly on the surface of APP for research on the flame retardancy and thermal conductivity of EP. By precisely controlling multiple deterministic parameters of the assembly, we were able to control the assembly density of CNTs on the surface of APP, and establish a uniform and fixed ordered thermal conductivity network based on the dispersion of the filler, thereby enhancing the flame retardant and thermal conductivity properties. Based on the aforementioned findings, a reasonable and well-founded explanation for the

superior properties exhibited by the composite materials prepared using this strategy was provided. This study emphasizes the potential for precise control of the self-assembly behavior of fillers at the nanoscale level, laying the foundation for the development of high-performance polymer materials.

2. Results and discussion

2.1. Morphology and structure of CNTs@APP

Figure 1a illustrates the synthesis of CNTs@APP through the ultrasound-assisted self-assembly of carboxylated CNTs onto the surface of APP. The key to creating CNTs@APP is the surface modification of CNTs with long-chain molecular ligands, enabling the formation of stable dispersions in organic solvents, essential for assembly[33]. As shown in **Figure S1**, the OAm moieties can be grafted onto the surface of the CNTs through hydrogen bonding between carboxyl and amine groups[34], allowing for their easy transfer from the aqueous phase to n-hexane **(Figure 1b and S2a-d)**. Subsequently, during the ultrasonic process, the colloidally stable CNTs are assembled onto the APP surface through interfacial interactions, with OAm leaving from the surface of CNTs during the process due to the existence of antisolvent, labeled as CNTs@APP. It is important to note that the triggering of this assembly process is closely related to the choice of solvent system for assembly. When selecting a dual-phase system containing isopropanol and n-hexane—two solvents that are immiscible with each other—to create the conditions for assembly, the components dispersed in the two solvents intermingle to achieve the desired assembly upon ultrasonic assembly. Moreover, with isopropanol acting as an antisolvent for OAm[35], the presence of OAm as a ligand on the surfaces of CNTs could potentially compromise the flame retardancy and thermal conductivity. This is in contrast to the significant phase separation that would occur if only one solvent was selected and directly treated with ultrasound (**Figures S2e-f and S3**). This results in a reduction of the total system energy, with van der Waals forces and hydrogen bonding playing significant roles in stabilizing such structures[36, 37], which are widely used in the preparation of such core-satellite

superstructure materials. In order to verify the effectiveness of this method and to regulate the thermal conductivity of flame retardant materials, we prepared a series of CNTs@APP by adjusting the mass ratio of CNTs to APP during feeding. Digital images of the assembled product reveal that the resulting CNTs@APP powder is gray, with the color deepening progressively as the ratio of CNTs to APP is increased (e.g., 1:50, 1:10, to 1:5), as shown in **Figure 1b** and **Figures S3c-e**, which is consistently intermediate between the white of APP and the black of CNTs (**Figures S4**), indicating no phase separation. Unlike other reported traditional methods where surface-modifying agents remain on the final product, this approach allows for the avoidance of introducing surface modifiers that may affect the properties of the material. This method demonstrates that by clever design, it is possible to prepare composite materials with superior comprehensive performance.

To verify the above assembly process and analyze the assembled CNTs@APP, the intermediate products of the process were carefully monitored using FTIR analyses, and the assembled products were thoroughly characterized using techniques such as TGA, XRD and SEM. Detailed tracking of the surface modification and assembly processes was conducted using infrared spectroscopy. The FTIR spectrum of the OAm-treated CNTs, presented in **Figure 1c**, shows distinct C-H stretching vibrations in the 2800-3000 cm^{-1} range, indicating the presence of OAm molecules[38]. Moreover, the appearance of N-H vibrations at 3320 cm^{-1}, along with the disappearance of O-H vibrations at 3440 cm^{-1}, implies an interaction between the OAm molecules and the surface carboxyl groups of the CNTs[34]. As the assembly process occurs, the characteristic peak of OAm disappears, while the characteristic peaks of CNTs and APP appear, indicating that the assembly is taking place and that OAm is leaving during the process. It is worth noting that after the assembly process, CNTs can stably exist on the surface of APP, likely driven by van der Waals forces. From this, it can be seen that during the assembly process, there is indeed a process of ligand introduction and detachment, which effectively promotes the assembly of CNTs on the surface of APP without any negative impact on the material's performance. Further, SEM images reveal

that CNTs@APP exhibit a superstructural morphology, with the CNTs uniformly distributed on the surface of APP (**Figure 1d-f**) and the morphology of the CNTs remains essentially unchanged after the treatment (**Figure S5**). This uniform distribution is further corroborated by EDS mapping images (**Figure 1g, S6**), particularly by the carbon element's contour, which closely matches the morphology of APP (**Figure S5a**), due to the carbon elements are not part of the molecular structure of APP. Together, the XRD patterns of CNTs@APP in **Figure S7** show that, regardless of the mass ratio of CNTs and APP, they exhibit the characteristic absorption peaks of both APP and CNTs, providing a clear explanation of their composition and structure. By the way, by adjusting the mass ratio of CNTs and APP, the distribution density of CNTs on the surface of APP can be well controlled. The more CNTs added, the denser the distribution of CNTs on the surface of APP (as shown in **Figure 1b, S8 and S9**), which seems to be conducive to the construction of a denser thermal conductivity network. It is worth noting that excessive introduction of CNTs may affect its flame retardant performance.

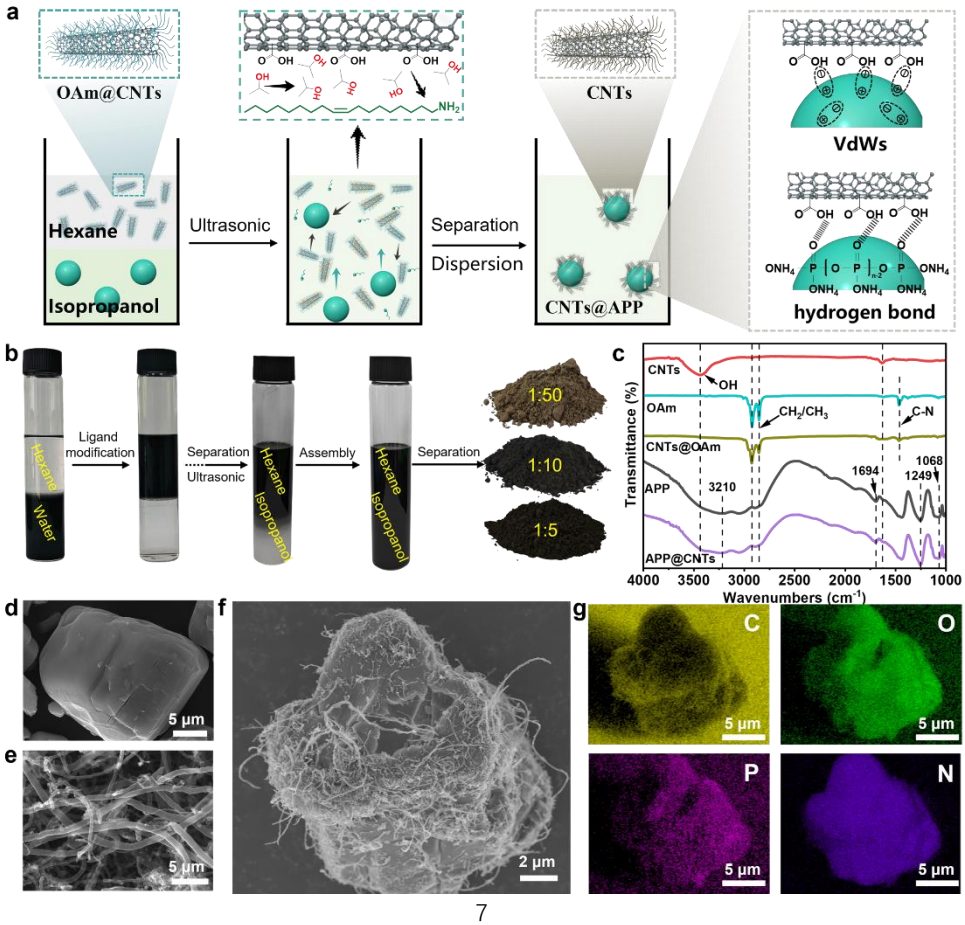

Figure 1. Design and synthesis of CNTs@APP nanohybrid. (a) Synthetic route of CNTs@APP nanohybrid, (b) Photographs and (c) FTIR spectra of CNTs and APP before and after ligand modification and self-assembly, respectively. Typical SEM images of (d) APP, (e) CNTs, (f) CNTs@APP, and (g) EDS mappings of CNTs@APP nanohybrid.

2.2. Combustion behavior of EP and its composites

The flame retardant properties of the EP nanocomposites prepared in this study (**Table S1**) were comprehensively evaluated using three different tests: the LOI, UL-94 vertical burning, and cone calorimeter tests. The UL-94 and LOI tests assessed the flammability of EP and its composites, with the summarized findings presented in **Figure 2a**. The LOI value of pure EP is 26.5%, almost the same to the reports, the lowest among all samples, indicating the high flammability of the unmodified EP[39]. However, the incorporation of flame retardants into the EP nanocomposites led to a noticeable improvement in LOI values. Comparing the results of composites with 7.5 wt% of different types of flame retardants, it was found that while APP alone could increase the LOI to 29.5% (EP-2), this enhancement was generally less than that observed in samples that incorporated CNTs (EP-3~EP-6), highlighting the significant role of CNTs in improving flame retardant performance. Notably, EP-4 exhibited a relatively lower LOI value of 28.6%, primarily because the higher proportion of CNTs in the sample resulted in a correspondingly lower amount of APP being added for an equivalent mass of flame retardant. Of particular interest is EP-5, which not only reached an LOI of 31.8% but also achieved a satisfactory UL-94 V-0 rating. This improvement compared to EP-3 can be attributed solely to the significant difference made by the self-assembly of CNTs on the surface of APP, which replaced simple blending. Additionally, by increasing the CNTs@APP flame retardant content from 5 wt% to 10 wt%, the LOI values of the EP nanocomposites gradually increased, which also enabled a transition from a UL-94 rating of V-1 to V-0. It is evident that both the LOI values and UL-94 ratings show a clear positive correlation with the amount of

flame retardant added, demonstrating the effectiveness of CNTs@APP as a flame retardant.

Cone calorimetry has been widely recognized as an effective tool to study the actual combustion behavior of polymers in large-scale fires[40, 41]. The relevant data for EP and its composites are displayed in **Figure 2b-i** and summarized in **Table S2**. As shown in **Table S2**, nearly all EP samples exhibited ignition times similar to that of pure EP, suggesting that the added flame retardants are well-compatible with the resin, a compatibility that relates directly to their modest addition amounts. It's important to note that the pure EP burned with high peak heat release rate (PHRR) of 979 kW/m^2 and total heat release (THR) of 85.2 MJ/m^2, which are among the highest values for all the samples tested. After the addition of flame retardants, particularly with the measured introduction of small amounts of CNTs via assembly, these values significantly decreased. For example, the PHRR values of EP-4 and EP-7 decreased by 45.6% and 37.2%, respectively. Especially noteworthy is when the blended CNTs/APP in EP-3 is replaced with the assembled CNTs@APP in EP-5, resulting in a marked reduction in all major flammability metrics for the EP nanocomposites, such as THR (46.1 MJ/m^2), total smoke release (TSR) (1724 m^2/m^2), and total smoke production (TSP) (15.2 m^2/s), all dropping by more than 30%. Moreover, compared to pure EP (EP-1), these reductions ranged from 45.9% to 56.9% (**Figure 2c, 2e and 2f**), underscoring the dramatic improvement in fire safety afforded by the assembled CNTs@APP. Moreover, the peak intensity of CO yield (PCOY) dramatically decreased from 17.12 kg/kg to 3.86 kg/kg, marking a substantial reduction of 77.5% (**Table S2**). This significant decrease suggests that the inclusion of CNTs@APP not only enhances the flame retardancy but also offers a considerable advantage in controlling harmful emissions. This improvement is likely due to the superior dispersion of CNTs@APP within the resin, which promotes more complete combustion of the material. Additionally, the beneficial effects continue to amplify with the increased concentration of CNTs@APP and the proportion of CNTs within the CNTs@APP composite, from EP-4 through EP-8 samples. However, it is important to note that an excessive addition of flame retardants

can negatively impact the material's inherent properties. Therefore, achieving a balance between enhanced flame retardancy and the preservation of material characteristics is crucial for practical applications. Suddenly, we found that the PHRR and THR values for EP-2 were abnormally higher than those for pure EP, which may be due to the inhomogeneous mixing of APP with EP, potentially forming localized enrichment areas within the resin. These areas might exhibit abnormal combustion characteristics, which could be directly related to the hygroscopic nature of APP itself. When APP and CNTs are simply blended, two distinct peaks appear in the HRR curve. However, with CNTs assembled on the surface of APP, only one peak is observed. The initial peak could result from APP decomposing to release phosphoric acid and water, which promotes the formation of a protective char layer. As the temperature rises, the EP's decomposition intensifies, causing the second peak. In the case of simple blending, the uneven distribution of APP and CNTs can cause localized variations in flame retardant efficiency, leading to multiple peaks during combustion. Conversely, with CNTs assembly, a more uniform dispersion and improved compatibility at the microlevel lead to more consistent thermal decomposition reactions. Moreover, the presence of CNTs aids in the formation of a more complete char layer, which acts as an effective barrier during combustion, thereby significantly reducing THR despite a high PHRR. This indicates that although the assembled flame retardant doesn't completely prevent heat release initially, it effectively suppresses further heat and mass loss later in the combustion process. The rapid formation of a stable char layer early in the combustion process contributes to a substantial reduction in heat and smoke emission.

The formation of char is one of the key protective mechanisms for polymer materials under fire conditions[42]. By creating a carbonaceous barrier layer during the pyrolysis process, effective insulation against heat and oxygen transfer can be achieved, which in turn reduces the combustion rate of the material and enhances its flame retardant performance. **Figure 2i** presents the statistical graph of the char yield for various EP nanocomposites after combustion. From the graph, it is apparent that EP-1 has the lowest char yield at only 9.85% among all samples. Upon the introduction of

flame retardants, the char yields for samples EP-2 to EP-8 exhibited a marked increase. Notably, the inclusion of assembled CNTs@APP (EP-5) led to a remarkable char yield of 45.49%, which is a 3.6-fold increase in comparison to EP-1. While the addition of flame retardants does have some impact on the increase of char yield, a detailed comparison reveals that this is not the sole determining factor. For example, both EP-3 and EP-5 had identical amounts of flame retardant added, with the only difference being that EP-5 contained assembled CNTs@APP, while the latter incorporated the retardants via simple blending. The char yield of EP-5 was nearly 30.9% higher than that of EP-3. Besides, the difference between EP-5 and EP-6 lies in the proportion of CNTs in the CNTs@APP—10% for EP-5 and only 2% for EP-6. Despite the lesser amount of carbon material introduced in EP-6, its char yield increased to 47.7%. This may be attributed to the relatively lower coverage of APP by CNTs, allowing the APP to decompose more thoroughly upon heating and to release acidic substances[43]. These substances can catalyze the carbonization process of the EP, hence forming a more substantial char layer. This indicates that the selection of an appropriate flame retardant and its method of preparation play a crucial role in fully leveraging its flame-retardant efficacy.

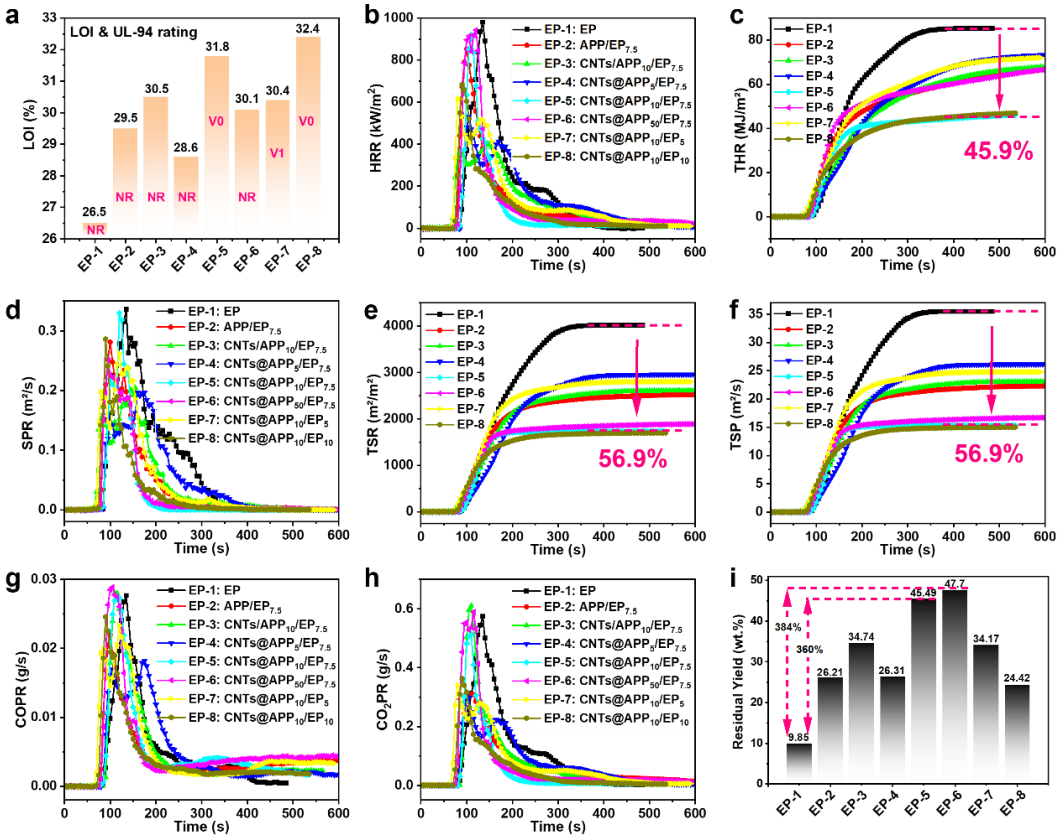

Figure 2. (a) UL-94 results and LOI value, (b) HRR, (c) THR, (d) SPR, (e) TSR, (f) TSP, (g) COPR, (h) CO_2PR curves and (i) residual yield of EP and its composites.

To further understand the flame retardant mechanism of complex flame retardants, we conducted a detailed analysis of the morphology and graphitization degree of the char layer of samples of EP and its composites after cone calorimetry testing using digital cameras, SEM, and Raman spectroscopy. The relevant results are shown in **Figure 3**. As shown in **Figures 3a$_1$ and 3b$_2$**, the EP-1 has been almost completely burned after cone calorimetry testing, leaving only a small amount of charred residue, with many large holes on the surface of the remaining char layer (**Figure 3a$_1$-d$_1$**), which is why it cannot suppress heat release and smoke generation, resulting in poor flame retardancy and smoke inhibition performance of EP/DDM. The charred situation of EP-2 is almost the same as EP-1, with many cracks on the surface of the residual char (**Figure 3a$_2$-d$_2$**). However, introducing CNTs into the system has brought about significant changes. Simply adding about 0.75 wt% of CNTs to the system has greatly

increased the expansion degree of the residual char, almost doubling the expansion degree compared to before the addition (**Figure 3a$_3$-d$_3$**). Unfortunately, at this point, the surface of the residual char layer still contains some small holes, which is the direct reason for its poor flame retardant performance. These unfavorable conditions have changed significantly after assembling CNTs on the surface of APP instead of simple blending (**Figure 3a$_4$-d$_8$**). The most obvious change is that the sample of EP composite material with added CNTs@APP flame retardant forms a continuous dense char layer after burning (**Figure 3d$_4$-d$_8$**), which cannot be achieved through direct blending (**Figure 3d$_1$-d$_3$**). This is directly verified by the multi-layered char layers shown in the cross-section of the char residue (**Figure S10**) and SEM images of the char layer at various locations, all of which show a continuous and dense char layer (**Figure S11**). Although the morphology of the inner residual char layers characterized by SEM is similar, there is still a significant difference in the expansion degree of the char layer (**Figure 3a$_4$-a$_8$**) and morphology of the outer residual char layers (**Figure 3c$_4$-c$_8$**). As shown, the expansion degree of the residual char increases and then decreases with the increasing proportion of CNTs in CNTs@APP in EP-4, EP-5 and EP-6 (1:5, 1:10, and 1:50), with the maximum expansion degree at 1:10, increasing to about 4 times the expansion degree of EP-1 and EP-2 (~60 mm). This indicates that the content of CNTs in flame retardants has a significant effect on the expansion effect of expansion-type flame retardants, and the appropriate proportion of CNTs directly contributes to the construction of a dense insulation layer, thereby achieving a greater expansion degree. When the content of CNTs is too high, the proportion of APP in the flame retardant system decreases, leading to a decrease in the expansion degree of the char layer (~31 mm). Additionally, when investigating the effect of the amount of flame retardant, we find that the expansion degree of the residual char almost increases with the increasing flame retardant. For example, comparing **Figures 3a$_7$ and 3a$_8$**, it is evident that when the amount of CNTs@APP flame retardant added is 5% and 10%, the height of the residual char also increases from 22 mm to 52 mm, achieving an increase of nearly 2.36 times, indicating a direct effect of the amount of flame retardant on the expansion

situation of the residual char layer, which perfectly echoes the above flame retardancy test. Of course, by comparing EP-5 and EP-8, when the amount of CNTs@APP flame retardant is increased from 7.5% to 10%, the expansion degree of the residual char actually decreases to some extent, from 60 mm to 52 mm. Apart from the deviations caused by the tests, this is also due to adding too much CNTs@APP_{10} causing it to be distributed more widely in the EP resin, resulting in the polymer chain in the resin being less densely distributed, affecting the formation of an effective dense char layer during combustion, and thus affecting the expansion effect of the char layer.

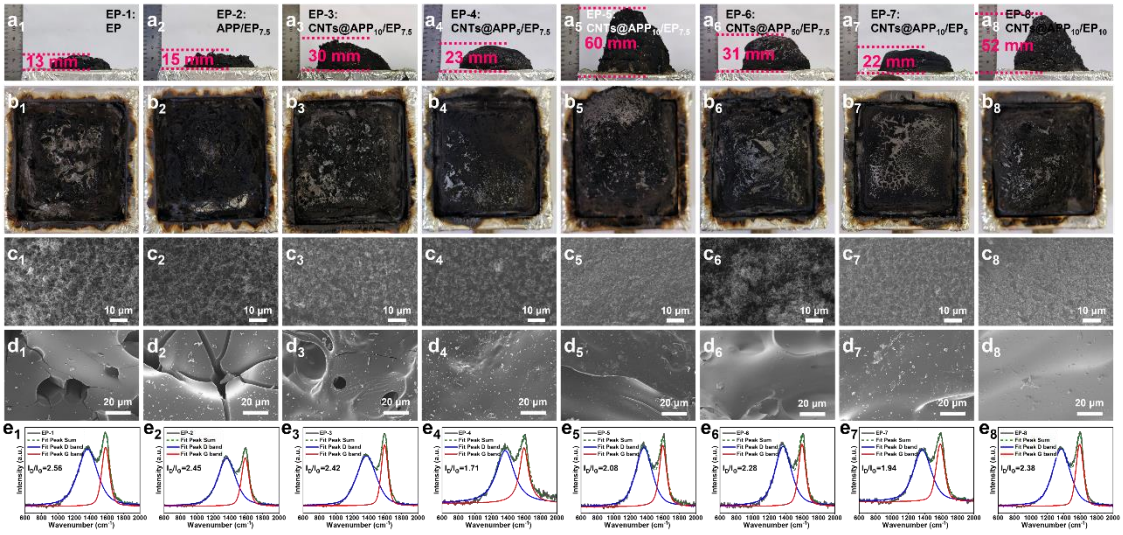

Figure 3. (a_1-a_8, b_1-b_8) Photographs, (c_1-c_8, d_1-d_8) SEM images and (e_1-e_8) Raman spectra of EP and its nanocomposites, (a_1-a_8) side view, (b_1-b_8) top view, (c_1-c_8) the external and (d_1-d_8, e_1-e_8) internal char layer.

Further analysis of the Raman spectra of the char residues (**Figures 3e1-e8**) revealed that all char residues showed D and G peaks at about 1350 and 1600 cm^{-1}, respectively, corresponding to disordered carbon structures and graphitized structures. The ratio of the integrated areas of the D and G peaks (I_D/I_G) reflected the degree of graphitization of the char residues, with a lower I_D/I_G indicating a higher degree of graphitization and better thermal stability. The I_D/I_G value of the EP-1 sample char residue was almost the highest among all the EP samples (**Figures 3e1,** I_D/I_G=2.56), indicating the lowest degree of graphitization and the poorest thermal stability. Similarly, the I_D/I_G values of EP-2 and EP-3 samples containing only APP or a

combination of CNTs and APP were also relatively high, suggesting average graphitization levels (**Figures 3e$_2$-3e$_3$)**. In contrast, the I_D/I_G values of the EP samples (EP-4~EP-8) containing the assembled flame retardant, CNTs@APP, showed a noteworthy decrease, with the highest graphitization achieved at a CNTs:APP ratio of 1:5 (**Figures 3e$_4$**). Deviations from this ratio resulted in differences, indicating a direct relationship between the appropriate ratio of CNTs to APP and improved graphitization degree. This could be due to the assembly of an appropriate proportion of CNTs on the surface of APP, which in the subsequent combustion process would create a denser char layer through mutual CNTs construction[44], leading to local heat retention and promoting an increase in graphitization degree.

2.3. Thermal conductivity performance of EP and its nanocomposites

To investigate the thermal conductivity performance of EP and its nanocomposites, we measured the thermal conductivity coefficients of the materials using a Hot Disk thermal conductivity analyzer employing the transient plane source method. Simultaneously, we recorded the relationship between temperature and heating time of the EP nanocomposites in real-time using infrared thermal imaging, with the results presented in Figure 4. As depicted in **Figure 4a**, the neat EP (EP-1) exhibited the lowest thermal conductivity coefficient at approximately 0.207 W $m^{-1}K^{-1}$, which is directly associated with its amorphous nature. The addition of APP flame retardant resulted in a slight increase in the thermal conductivity coefficient (EP-2), but the improvement was modest. A significant enhancement was seen with the introduction of 0.75 wt% CNTs, which increased the thermal conductivity coefficient to 0.268 W $m^{-1}K^{-1}$ (EP-3); however, the degree of improvement was not substantial. When the assembled thermally conductive flame-retardant filler CNTs@APP was added (EP-4, EP-5, and EP-6), a notable increase in the thermal conductivity of the EP nanocomposites was observed. Nevertheless, among these three samples, the thermal conductivity decreased significantly with the reduction of CNTs content. Notably, EP-4's thermal conductivity coefficient increased to 0.317 W $m^{-1}K^{-1}$, a nearly 53% enhancement compared to pure

EP. While the result may not seem superior in comparison to the literature, it should be noted that the added CNTs content was considerably less than the thermal filler quantities reported in other studies[45, 46]. It is particularly noteworthy that EP-3 and EP-5, despite having identical compositions, exhibited different thermal conductivities, with the latter being significantly higher, highlighting that substituting simple blends with assembled CNTs@APP is an effective approach to improve material thermal performance. Additionally, by comparing EP-7, EP-5, and EP-8, it is clear that there is a positive correlation between the amount of thermal filler added and the material's thermal conductivity. Nevertheless, this does not imply that excessive filler should be added to achieve high thermal conductivity, as this would necessitate consideration of cost (crucial for industrial production) and could also compromise the material's mechanical properties[47]. Simultaneously, to demonstrate the practical thermal diffusion behavior of EP and its nanocomposites, the surface temperature variations with time during heating were recorded by an infrared thermal imager, and the results are shown in **Figure 4b-c**. It can be observed that the surface temperatures of all samples increased continuously within a 420 s timeframe until reaching a saturated temperature, with the heating rate order being EP-1 < EP-2 < EP-6 < EP-7 < EP-3 < EP-5 < EP-8 < EP-4. This progression is consistent with the thermal conductivity results shown in Figure 4a. These findings illustrate that the CNTs@APP/EP nanocomposites possess excellent heat dissipation capabilities. With their high flame retardancy, the CNTs@APP/EP nanocomposites demonstrate promising potential for thermal management applications in scenarios where fire risk is a concern.

Based on the results of the thermal conductivity tests, the mechanism of heat dissipation for CNTs@APP flame-retardant fillers in an EP matrix is illustrated in **Figure 4d**. When the sample is placed on a preheated hot plate, heat begins to diffuse upward from the bottom of the sample. During this process, the thermally conductive fillers within the EP composite material transfer heat via phonon conduction. Notably, CNTs@APP flame-retardant fillers prepared by self-assembly exhibit a uniform dispersion of CNTs across the surface of the APP, resulting in a greater volume fraction

within the EP resin. More significantly, CNTs are not dispersed within the inter-filler resin, which might seem counterproductive for constructing conductive pathways. However, this facilitates the formation of thermal pathways as the CNTs on the surface of CNTs@APP are more likely to come into contact with each other. Furthermore, the carboxyl groups enriched on the surface of CNTs@APP promote enhanced heat transfer through the formation of hydrogen bonds and van der Waals interactions among the fillers, thereby forming a thermal conductive network throughout the EP matrix and achieving more rapid heat dissipation. Additionally, the carboxyl functional groups can participate in the curing process of the EP, firmly anchoring the CNTs@APP in the optimal position and ensuring that there is no filler migration that could affect thermal efficiency. As a result, composites with self-assembled CNTs@APP as thermal fillers demonstrate superior heat transfer properties within the EP matrix. In contrast, simply blending APP flame retardants and CNTs thermal fillers into the EP resin traditionally does not adequately leverage their synergistic potential, a conclusion supported by the previously mentioned lower flame retardancy efficiency. Worse still, due to the limited amount of CNTs added directly to the EP resin, it is difficult for the sparse CNTs to form an effective thermal pathway. Moreover, the challenge of uniformly dispersing APP within the resin, which tends to agglomerate, is detrimental not only to other properties such as flame retardancy but also to the formation of interconnected thermal conductive networks between fillers. The culmination of these adversities results in only moderate thermal conductivity of the EP nanocomposites prepared via blending. In summary, CNTs@APP/EP nanocomposites exhibit better thermal conductivity than pure EP and the EP nanocomposites with directly blended thermal fillers and possess potential applications in managing the thermal risks in electronic products.

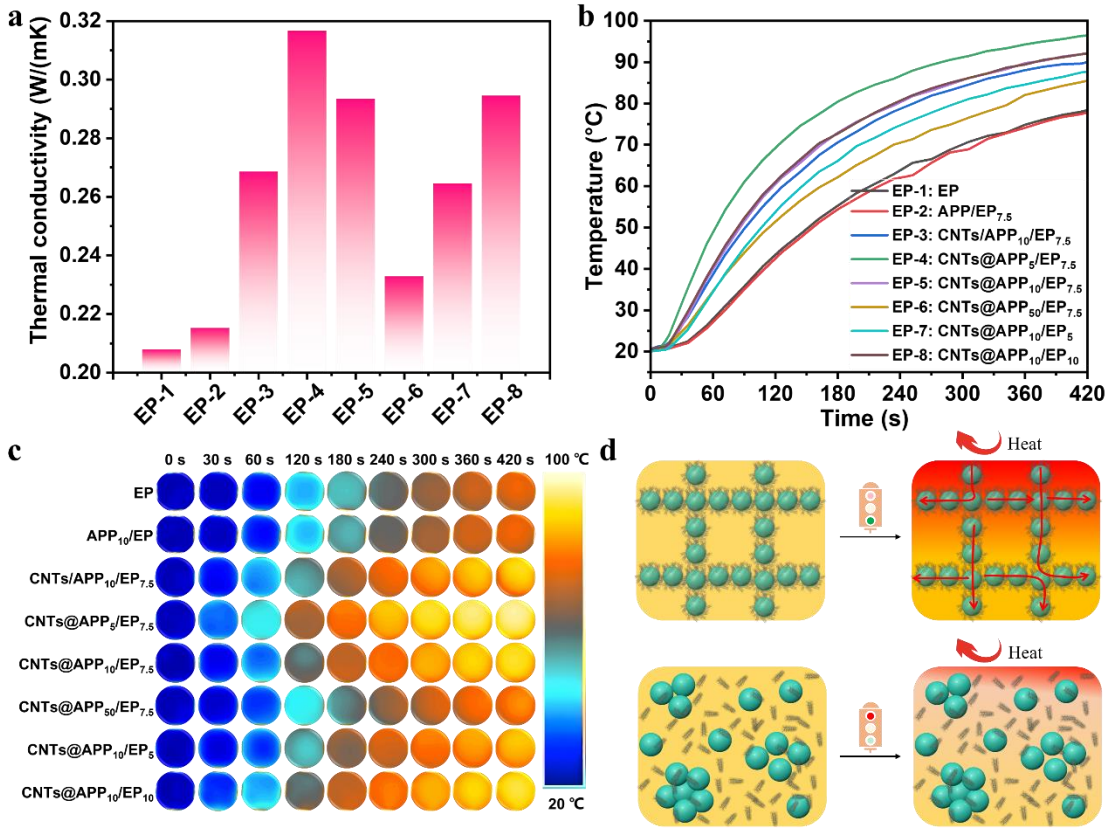

Figure 4. (a) The out-of-plane thermal conductivity of EP and its nanocomposites; (b) The changes in central temperature of the material surface over time during the heating process; (c) The infrared thermal images of EP and its nanocomposites during the heating process; (d) A graphical representation of the thermal conductivity mechanism for CNTs/APP/EP and CNTs@APP/EP nanocomposites.

2.4. Flame retardant and thermal conductive mechanism

Following meticulous analysis, we offer a cogent explanation for the mechanisms underlying the thermal conductivity and flame-retardant properties of CNTs@APP/EP nanocomposites (**Figure 5**). Initially, the uniform dispersion of a significant quantity of CNTs@APP dual-functional filler within the composite material is ensured by the presence of carboxyl functional groups on the surface of the CNTs. These groups not only facilitate the homogeneous distribution within the EP but also participate in the curing process of EP[48]. Consequently, after high-temperature curing, the filler is fixed in place, preventing migration in later stages. Moreover, the distinctive core-satellite structure of the composite dual-functional filler, with APP at the core and CNTs forming

the satellite, allows for a substantial volume fraction of CNTs in the matrix. Even a small quantity of CNTs, when dispersed in the EP matrix, is likely to contact one another, potentially creating a network-like pathway that enhances the material's thermal conductivity. Upon pyrolysis under heat flux, the CNTs tightly adhered to the APP surface in EP nanocomposites can efficiently and stably decompose into phosphorus oxide radicals and phosphorus-containing substances, such as polyphosphate. These byproducts can effectively capture the hydrogen and hydroxyl radicals produced by the thermal decomposition of EP, providing flame retardancy[18, 49]. Gaseous products like ammonia and water vapor also dilute the surrounding air, reducing the concentration of oxygen and contributing to flame retardancy[50]. During degradation of the hard segments, the polyphosphoric acid associated with CNTs@APP reacts with EP, dehydrating and crosslinking to rapidly form a dense and compact char layer. Additionally, the catalytic carbonization between CNTs and APP becomes more pronounced during burning, forming a protective char layer with a higher degree of graphitization, which effectively acts as a shield. It is noteworthy that under the same loading of fillers, the flame-retardant efficacy of CNTs@APP is superior to that achieved by simply blending APP with CNTs. This can be attributed to the even distribution of CNTs@APP within the EP and their secure anchoring, which are crucial for enhancing flame retardancy. Nonetheless, the thermal expansion of the EP matrix upon heating could increase the distance between the contacting CNTs, potentially reducing the composite's thermal conductivity. As the heat diffusion persists and APP continues to decompose, CNTs initially assembled on the surface of APP gradually deposit into the EP matrix. The continuous deposition and accumulation of CNTs create a dense cover layer on the surface of the resin, trapping the decomposition gases and causing them to circulate within the matrix, which promotes the surface expansion of the composite material and leads to a multilayered structure with discernible gaps, as clearly observed in Figure S2. With the ongoing expansion of the char layer, the distance between the contacting CNTs further widens, eventually disrupting their thermal conductive properties. Subsequently, the continuous formation of a dense char

layer isolates the remaining EP from air, extinguishing the flame and achieving excellent flame retardancy. In conclusion, the superior flame retardancy and thermal conductivity of the CNTs@APP/EP composite material stem from the uniform dispersion of CNTs@APP within the EP, effective contact between CNTs, and synergistic interactions among different components, all of which are essential to the underlying mechanism.

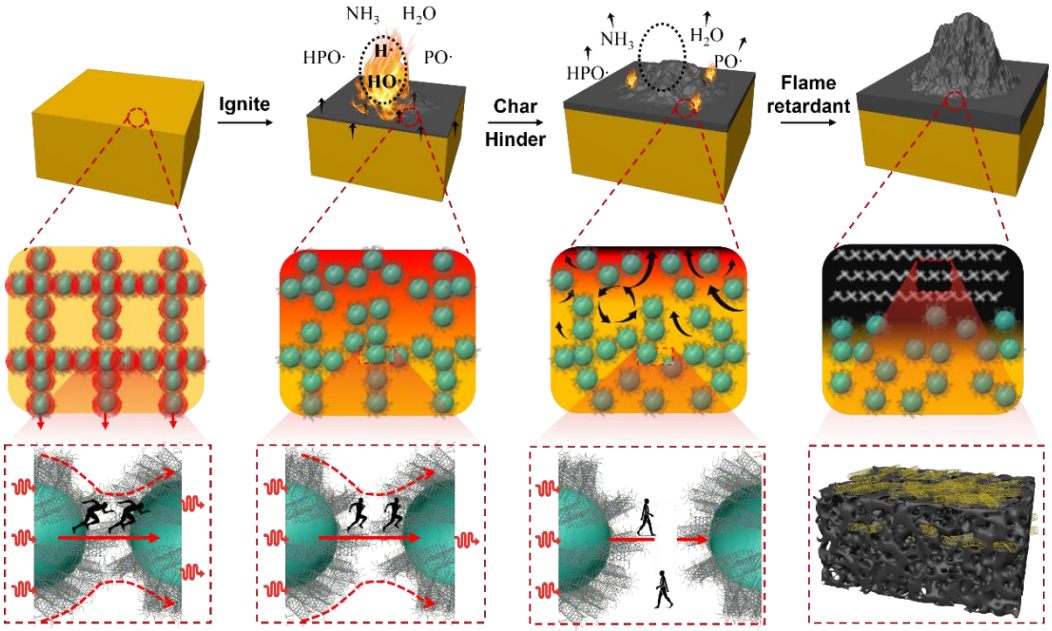

Figure 5. Schematic diagram of the possible thermal conductive and flame retardant mechanism for EP nanocomposites.

3. Conclusion

In this study, we have successfully synthesized a structurally optimized CNTs@APP nanohybrid through an ultrasound-assisted self-assembly process that is enhanced by ligand treatment and the careful selection of solvents. The resulting EP nanocomposites, which incorporates 7.5 wt% of the CNTs@APP$_{10}$, exhibits marked improvements in terms of flame retardancy and thermal conductivity when compared to pure EP. Specifically, the composite demonstrated a significant increase in the LOI of 31.8%, alongside marked reductions in THR, TSR, PCOY by 45.9%, 56.9% and 77.5%, respectively. These improvements enabled the composite to fulfill the UL-94 V-0 rating standards. Additionally, the thermal conductivity of the composite was

increased by almost 53%, thanks to the even distribution of the CNTs@APP and the creation of a structured thermal conductive network within the EP matrix. These findings underscore the effectiveness of nanoscale precision-controlled self-assembly of novel flame retardants in developing advanced high-performance flame retardant composite materials that are suitable for a broad spectrum of applications.

4. Experimental Section

Materials: Diglycidyl ether of bisphenol A (DGEBA, epoxide value: 0.53 mol/100 g) was procured from Yueyang Baling Huaxing Petrochemical Co., Ltd. located in Hunan, China. Isopropanol, hexane, ammonium polyphosphate (APP), and 4,4'-diaminodiphenylmethane (DDM) were sourced from Sinopharm Chemical Reagent Co., Ltd. based in Shanghai, China. Oleylamine (OAm, 70%) was purchased from Aldrich. Carboxylated carbon nanotubes (CNTs) were acquired from JiangNan Graphene Research Institute and were utilized in their pristine state without any further modification. Ultrapure water with a resistivity of 18.25 MΩ cm at 25 °C was used in all experiments.

Instruments and characterization: Scanning electron microscopy (SEM) and energy dispersive X-ray spectroscopy (EDS) analyses were conducted using a Zeiss Ultra-55 microscope, operated at 5 and 15 kV, respectively. X-ray diffraction (XRD) measurements were performed on a Bruker D4 X-ray diffractometer. Raman spectra were recorded on an XploRA Raman system at room temperature. Fourier-transform infrared (FTIR) spectra were obtained using a Thermo Scientific Nicolet iS20.

The LOI of the EP sample was tested on a PX-01-005 oxygen index instrument from Phinix, China, following the ASTM D2863 standard. The size of the sample was

130 × 6.5 × 3 mm³. The UL-94 classification of the EP samples was tested using a CZF-3 vertical combustion tester from Jiangning, China, based on the ISO-1210 standard. The size of the sample was 130 × 13 × 3 mm³. The flame retardancy of epoxy thermosets was further evaluated using an FTT-0242 cone calorimeter from Fire Testing Technology, UK, based on the ISO 5660 standard, with a heat flux of 35 kW/m². The size of the specimen was 100 × 100 × 3.0 mm³, and the reported data were the averages of three specimens.

The Hot Disk 2500 thermal analyzer, which uses Transient Plane Sources (TPS) technology, was used to measure the thermal conductivity. A heated panel from Thermo Scientific in the USA was used as the heat source at 100 °C, and an infrared camera from FLIR A400 in the USA was used to record temperature changes during the heating of composite samples with a diameter of 25 mm and a thickness of 8 mm.

Fabrication of CNTs@APP dual-functional filler by self-assembly: The preparation of CNTs@APP composite flame retardants consists of two main steps: surface modification of CNTs and assembly of modified CNTs on the surface of APP. Specifically, a typical experimental procedure for the assembly of CNTs and APP is described as follows:

In the first step, 100 mg of CNTs are dispersed uniformly in 20 mL of ultrapure water in a 60 mL glass bottle. Then, 20 mL of n-hexane (containing 0.01 mol/L oleylamine, OAm) is slowly added to the water surface. After appropriate shaking (taking care not to shake too vigorously), the CNTs are evenly coated with oleylamine

on the surface. The free OAm is removed by centrifugation and washing with n-hexane, resulting in OAm-modified CNTs, denoted as CNTs@OAm.

In the second step, 1 g of APP and the previously prepared CNTs@OAm are separately dispersed in a mixture of 20 mL isopropanol and n-hexane. The dispersions are then combined, followed by sonication for 2 hours or more until a homogeneous solution is obtained. Intense sonication facilitates the assembly of CNTs on the surface of APP (Note: due to the fact that isopropanol is a poor solvent for OAm, detachment of OAm from the surface of CNTs may occur during this process).

Finally, the resulting product is separated from the solvents by centrifugation at 5000 rpm for 5 minutes and then dried at 60°C. This product is referred to as CNTs@APP_{10}, where the number 10 represents the mass ratio of APP to CNTs used in this specific experimental procedure. Following this procedure, we obtained CNTs@APP_5, CNTs@APP_{10}, and CNTs@APP_{50}. It is worth mentioning that the described method can be easily scaled up by ensuring the volume of the sonication device and assembly container meet the experimental requirements.

Preparation of EP Composites: In the conventional protocol, CNTs@APP were directly incorporated into the EP matrix. The combination underwent mechanical stirring for 30 minutes at a temperature of 80°C. DDM was heated using a heating jacket until it reached a molten state at 120°C, after which it was added to the continuously stirred EP matrix. The mass ratio of EP to DDM was maintained at 100:26. The mixture was further mechanically stirred for 15 minutes at the same temperature. Subsequently,

the mixture was placed in a vacuum oven for 10 minutes and promptly transferred into a preheated polytetrafluoroethylene mold. To cure the resin, the mold was heated to 120℃ for 2 hours, followed by 160℃ for 2 hours. The final samples were labeled as CNTs@APP_x/EP_y, where 'x' represents the mass ratio of APP to CNTs used in the preparation of CNTs@APP and 'y' signifies the mass percentage of CNTs@APP in the EP matrix. As a control, we incorporated unassembled CNTs and APP into EP, denoted as CNTs/APP_x/EP_y, where 'x' represents the mass ratio of APP to CNTs and 'y' indicates the mass percentage of flame retardant in the composite material. For convenience, the formulations of EP composites with varying CNTs and APP content are summarized in Table S1. Additionally, pure EP and APP/EP were prepared using the same process.

Supporting Information

Supporting Information is available from the Wiley Online Library or from the author.

Acknowledgements

Y.X. and Y.H. contributed equally to this work. This work was supported by the National Natural Science Foundation of China (51973229, 51991355), the Scientific Research Foundation of NingboTech University (Grant No. 20220920Z0221), and the General Scientific Research Project of Zhejiang Education Department (No. Y202352936).

Conflict of Interest

The authors declare no conflict of interest.

Received: ((will be filled in by the editorial staff))
Revised: ((will be filled in by the editorial staff))
Published online: ((will be filled in by the editorial staff))

References

[1] A. Osman, A. Elhakeem, S. Kaytbay, A. Ahmed, *Adv. Compos. Hybrid Mater.* **2022**, *5*, 547.

[2] J. Yang, X. Shen, W. Yang, J. K. Kim, *Prog. Mater. Sci.* **2023**, *133*, 101054.

[3] Y. Wen, C. Chen, Y. Ye, Z. Xue, H. Liu, X. Zhou, Y. Zhang, D. Li, X. Xie, Y. W. Mai, *Adv. Mater.* **2022**, *34*, 2201023.

[4] J. Wang, Y. Liu, H. Zhao, J. Liu, D. Wang, Y. Song, Y. Wang, *Polym. Degrad. Stabil.* **2009**, *94*, 625.

[5] L. D. Mathews, J. C. Capricho, M. Peerzada, N. V. Salim, J. Parameswaranpillai, N. Hameed, *Mater. Today Commun.* **2022**, *33*, 104702.

[6] Q. Chen, L. Liu, A. Zhang, W. Wang, Z. Wang, J. Zhang, J. Feng, S. Huo, X. Zeng, P. Song, *Chem. Eng. J.* **2023**, *454*, 140424.

[7] P. Xue, Y. Cheng, Y. Wang, G. Han, B. Zhou, C. He, C. Liu, Y. Feng, *Chem. Eng. J.* **2023**, *474*, 145791.

[8] S. Lou, R. Yu, S. Wang, P. Fan, J. Liu, T. Tang, *Polymer* **2023**, *268*, 125715.

[9] G. Han, X. Zhao, Y. Feng, J. Ma, K. Zhou, Y. Shi, C. Liu, X. Xie, *Chem. Eng. J.* **2021**, *407*, 127099.

[10] Z. Sun, J. Li, M. Yu, M. Kathaperumal, C. Wong, *Chem. Eng. J.* **2022**, *446*, 137319.

[11] M. Zhou, G. Yin, S. G. Prolongo, D. Wang, *Polymers* **2023**, *15*, 2818.

[12] Y. Ouyang, L. Bai, H. Tian, X. Li, F. Yuan, *Compos. Pt. A-Appl. Sci. Manuf.* **2022**, *152*, 106685.

[13] W. Yang, R. Lin, X. Li, C. Li, Y. Wu, G. Zhang, X. Liu, S. Li, Y. Wang, *J. Energy Storage* **2023**, *66*, 107372.

[14] B. W. Liu, H. B. Zhao, Y. Z. Wang, *Adv. Mater.* **2022**, *34*, e2107905.

[15] K. Song, Y. Pan, J. Zhang, P. Song, J. He, D. Wang, R. Yang, *Chem. Eng. J.* **2023**, *468*, 143653.

[16] W. Wu Klingler, A. Bifulco, C. Polisi, Z. Huang, S. Gaan, *Compos. Pt. B-Eng.* **2023**, *258*, 110667.

[17] R. Lian, M. Ou, Z. Zhao, Q. Gao, X. Liu, L. Liu, X. Chen, C. Jiao, *Prog. Org. Coat.* **2023**, *183*, 107750.

[18] M. Wan, C. Shi, X. Qian, Y. Qin, J. Jing, H. Che, F. Ren, J. Li, B. Yu, K. Zhou, *Chem. Eng. J.* **2023**, *459*, 141448.

[19] R. Lian, M. Ou, H. Guan, J. Cui, Z. Zhao, L. Liu, X. Chen, C. Jiao, *Constr. Build. Mater.* **2023**, *389*, 131786.

[20] Q. Bao, R. He, Y. Liu, Q. Wang, *Compos. Pt. A-Appl. Sci. Manuf.* **2023**, *164*, 107309.

[21] H. Y. Zhao, M. Y. Yu, J. Liu, X. Li, P. Min, Z. Z. Yu, *Nano-Micro Lett.* **2022**, *14*, 129.

[22] T. Sai, S. Ran, Z. Guo, P. Song, Z. Fang, *SusMat* **2022**, *2*, 411.

[23] X. Bi, H. Di, J. Liu, Y. Meng, Y. Song, W. Meng, H. Qu, L. Fang, P. Song, J. Xu, *Adv. Compos. Hybrid Mater.* **2022**, *5*, 1743.

[24] Z. Yang, G. Xiao, C. Chen, C. Chen, F. Zhong, M. Wang, R. Zou, R. Li, Y. Li, M. Cao, *Prog. Org. Coat.* **2023**, *177*, 107426.

[25] Z. Li, Q. Fan, Y. Yin, *Chem. Rev.* **2022**, *122*, 4976.

[26] W. Wang, Y. Kan, J. Liu, K. M. Liew, L. Liu, Y. Hu, *J. Hazard. Mater.* **2017**, *340*, 263.

[27] E. Meirzadeh, A. M. Evans, M. Rezaee, M. Milich, C. J. Dionne, T. P. Darlington, S. T. Bao, A. K. Bartholomew, T. Handa, D. J. Rizzo, R. A. Wiscons, M. Reza, A. Zangiabadi, N. Fardian-Melamed, A. C. Crowther, P. J. Schuck, D. N. Basov, X. Zhu, A. Giri, P. E. Hopkins, P. Kim, M.

L. Steigerwald, J. Yang, C. Nuckolls, X. Roy, *Nature* **2023**, *613*, 71.
[28] C. Zhang, W. Lu, Y. Xu, K. Zeng, G. W. Ho, *Nature* **2023**, *616*, 293.
[29] F. X. Redl, K. S. Cho, C. B. Murray, S. O'Brien, *Nature* **2003**, *423*, 968.
[30] C. Wang, K. Gong, B. Yu, K. Zhou, *Compos. Pt. B-Eng.* **2023**, *265*, 110935.
[31] L. Yin, K. Gong, K. Zhou, X. Qian, C. Shi, Z. Gui, L. Qian, *J. Colloid. Interface. Sci.* **2022**, *608*, 853.
[32] X. Wang, S. Zhou, W. Xing, B. Yu, X. Feng, L. Song, Y. Hu, *J. Mater. Chem. A* **2013**, *1*, 4383.
[33] F. Zhang, J. Luo, J. Chen, H. Luo, M. Jiang, C. Yang, H. Zhang, J. Chen, A. Dong, J. Yang, *Angew. Chem. Int. Ed. Engl.* **2023**, *62*, e202310383.
[34] D. Han, Q. Zhou, Y. Xia, D. Huang, J. Qin, L. Wang, X. Wang, X. Zheng, D. Wu, *Carbon (New York)* **2022**, *200*, 296.
[35] Y. Hu, Y. Li, L. Yu, Y. Zhang, Y. Lai, W. Zhang, W. Xie, *Chem. Sci.* **2022**, *13*, 11792.
[36] Y. Liu, P. Zhang, N. Sun, B. Anasori, Q. Zhu, H. Liu, Y. Gogotsi, B. Xu, *Adv. Mater.* **2018**, *30*, 1707334.
[37] K. C. Kao, A. C. Yang, W. Huang, C. Zhou, E. D. Goodman, A. Holm, C. W. Frank, M. Cargnello, *Angew. Chem. Int. Ed. Engl.* **2021**, *60*, 2.
[38] Q. Cai, J. Wang, Y. Jiao, T. Li, Y. Xia, M. Li, Y. Yang, G. Wu, J. Zou, J. Hu, A. Dong, D. Yang, *Small* **2021**, *17*, 2101173.
[39] S. Huo, P. Song, B. Yu, S. Ran, V. S. Chevali, L. Liu, Z. Fang, H. Wang, *Prog. Polym. Sci.* **2021**, *114*, 101366.
[40] Q. Chen, L. Liu, A. Zhang, W. Wang, Z. Wang, J. Zhang, J. Feng, S. Huo, X. Zeng, P. Song, *Chem. Eng. J.* **2023**, *454*, 140424.
[41] M. Zhu, L. Liu, Z. Wang, *J. Hazard. Mater.* **2020**, *392*, 122343.
[42] K. Zhou, K. Gong, F. Gao, L. Yin, *Compos. Pt. A-Appl. Sci. Manuf.* **2022**, *157*, 106912.
[43] T. Zhang, H. Yan, M. Peng, L. Wang, H. Ding, Z. Fang, *Nanoscale* **2013**, *5*, 3013.
[44] J. Li, B. Hu, K. Hui, K. Li, L. Wang, *Compos. Pt. A-Appl. Sci. Manuf.* **2021**, *150*, 106633.
[45] C. Zhao, Y. Li, Y. Liu, H. Xie, W. Yu, *Adv. Compos. Hybrid Mater.* **2023**, *6*, 27.
[46] X. Tan, Q. Yuan, M. Qiu, J. Yu, N. Jiang, C. Lin, W. Dai, *J. Mater. Sci. Technol.* **2022**, *117*, 238.
[47] D. X. Sun, T. Gu, Y. T. Mao, C. H. Huang, X. D. Qi, J. H. Yang, Y. Wang, *Biomacromolecules* **2022**, *23*, 1789.
[48] A. Dabaleh, A. Mohammadi, A. Shojaei, A. Nematollahzadeh, *ACS Appl. Mater. Interfaces* **2024**, *16*, 5075.
[49] T. Mukhtar, R. Z. A. Manj, I. A. Khan, Z. A. Raza, M. Aslam, *Mater. Today Commun.* **2024**, *38*, 108208.
[50] P. Sun, P. Jia, W. Wang, N. Hong, F. Yu, D. Chen, B. Wang, Z. Gui, Y. Hu, *Compos. Pt. B-Eng.* **2024**, *279*, 111450.

Utilizing an innovative approach, a novel dual-functional filler comprising carbon nanotubes and ammonium polyphosphate (CNTs@APP) is created through a simple, ultrasound-assisted self-assembly technique. Distinguished from traditional blending methods, this precise technique significantly enhances flame retardancy and thermal conductivity in EP nanocomposites. This innovative approach offers promising advancements for high-performance applications in various industries.

Yan Xia, Yutong Hong, Li Zhang, Juan Chai, Bingtao Wang, Zhenghong Guo, Juan Li*, Siqi Huo*, and Zhengping Fang

Controllable Self-assembly of Carbon Nanotubes on Ammonium Polyphosphate as a Game-Changer for Flame Retardancy and Thermal Conductivity in Epoxy Resin

ToC figure